


SHORT REPORT

Open Access



# Landslide damage along Araniko highway and Pasang Lhamu highway and regional assessment of landslide hazard related to the Gorkha, Nepal earthquake of 25 April 2015

Chong Xu<sup>1\*</sup> , Yingying Tian<sup>1</sup>, Bengang Zhou<sup>1</sup>, Hongliu Ran<sup>1</sup> and Gaohu Lyu<sup>2</sup>

## Abstract

**Background:** The Gorkha, Nepal Mw 7.8 earthquake of 25 April 2015 triggered a large number of coseismic landslides in a broad area. Two highways, Araniko Highway and Pasang Lhamu Highway, that connect Tibet of China and Nepal, were affected seriously by these landslides. The purpose of this study was to investigate the landslide damage along the two highways, construct a detailed and complete inventory of coseismic landslides in the 5-km buffer area of the Araniko Highway, and perform a regional assessment of landslide hazard in the affected area.

**Findings:** Based on visual interpretation of high-resolution satellite images, field investigations, and GIS technology, we investigated the coseismic landslides along the Araniko Highway and Pasang Lhamu Highway. A detailed point-based inventory of coseismic landslides was constructed and spatial distributions of the landslides were analyzed. Correlations between the landslides and five controlling factors, i.e. elevation, slope angle, slope aspect, lithology, and seismic intensity, were illustrated statistically which permitted to assess landslides hazard in a larger rectangle area.

**Conclusions:** We examined the coseismic landslides of the 2015 Gorkha earthquake that blocked or damaged the Araniko Highway (117.3 km) and Pasang Lhamu Highway (139.3 km) in Nepal. Results show 35 coseismic landslides damaged the Araniko Highway along a total length 1,415 m. The total volume of them was estimated to be 0.37 million m<sup>3</sup>. We delineated 89 coseismic landslides that damaged the Pasang Lhamu Highway, where the total length of the damaged or buried roads is about 2,842 m and the total volume of the 89 landslides is about 1.47 million m<sup>3</sup>. In the 5-km buffer area along the Araniko Highway, we mapped 3,005 landslides caused by the Gorkha earthquake. The landslide number density of the study area is 2.925 km<sup>-2</sup>. The places with elevations 2,000–2,500 m have the highest landslide concentration. Landslide number density values increase with the slope angle. The slope aspects E and SE correspond to the highest concentrations of coseismic landslides. The underlying bedrock of Precambrian rocks-1 (Pc1) registered the largest landslide number density. The area of seismic intensity IX has a much higher LND value than that of the intensity VIII. We used the weigh index method to perform landslide hazard assessment in the 5-km buffer area on either side of the highway, which shows a success ratio of 85.9%. This method has been applied to a larger area mainly encompassing Rasuwa and Sindhupalchok counties of Nepal.

**Keywords:** Gorkha earthquake, Coseismic landslides, Field investigation, Visual interpretation, Landslide hazard assessment

\* Correspondence: xuchong@ies.ac.cn

<sup>1</sup>Key Laboratory of Active Tectonics and Volcano, Institute of Geology, China Earthquake Administration, 1# Huayanli, Chaoyang District, PO Box 9803, Beijing 100029, China

Full list of author information is available at the end of the article

**Introduction**

The 25 April 2015 Gorkha, Nepal Mw 7.8 earthquake caused more than 8,800 fatalities and enormous economic losses. It also triggered a large number of coseismic landslides, mainly shallow and disrupted landslides and a few deep-seated landslides, some of which buried villages, roads, and valleys (Hashash et al. 2015; Moss et al. 2015; Dahal 2016; Gnyawali et al. 2016; Martha et al. 2016; Wang et al. 2016; Xu et al. 2016a). The affected areas include Central Nepal and Gyirong and Nielamu counties of southern Tibet, China. The coseismic landslides seriously damaged two highways, Pasang Lhamu Highway and Araniko Highway, connecting China and Nepal. After the event, several research teams carried out field investigations of seismic damages and earthquake-triggered landslides (Collins and Jibson 2015;

Hashash et al. 2015; Sun and Yan 2015; Kargel et al. 2016; Lacroix 2016; Sharma et al. 2016). Until now, however, little work focuses on the landslides that damaged these two highways. Although the materials of the coseismic landslides blocking the two main roads have been cleaned up in time, some new landslides were triggered by aftershocks or strong rainfalls, resulting in further damage. Therefore, identifying the landslides destroying the roads and assessment of landslide hazard is very important for prevention and mitigation of future geologic hazard around these two roads. In this work, we firstly identified the coseismic landslides that destroyed the Lhamu Highway and Araniko Highway using field investigation and visual interpretation of satellite images. Then we constructed a detailed inventory map containing 3,005 individual coseismic landslides in

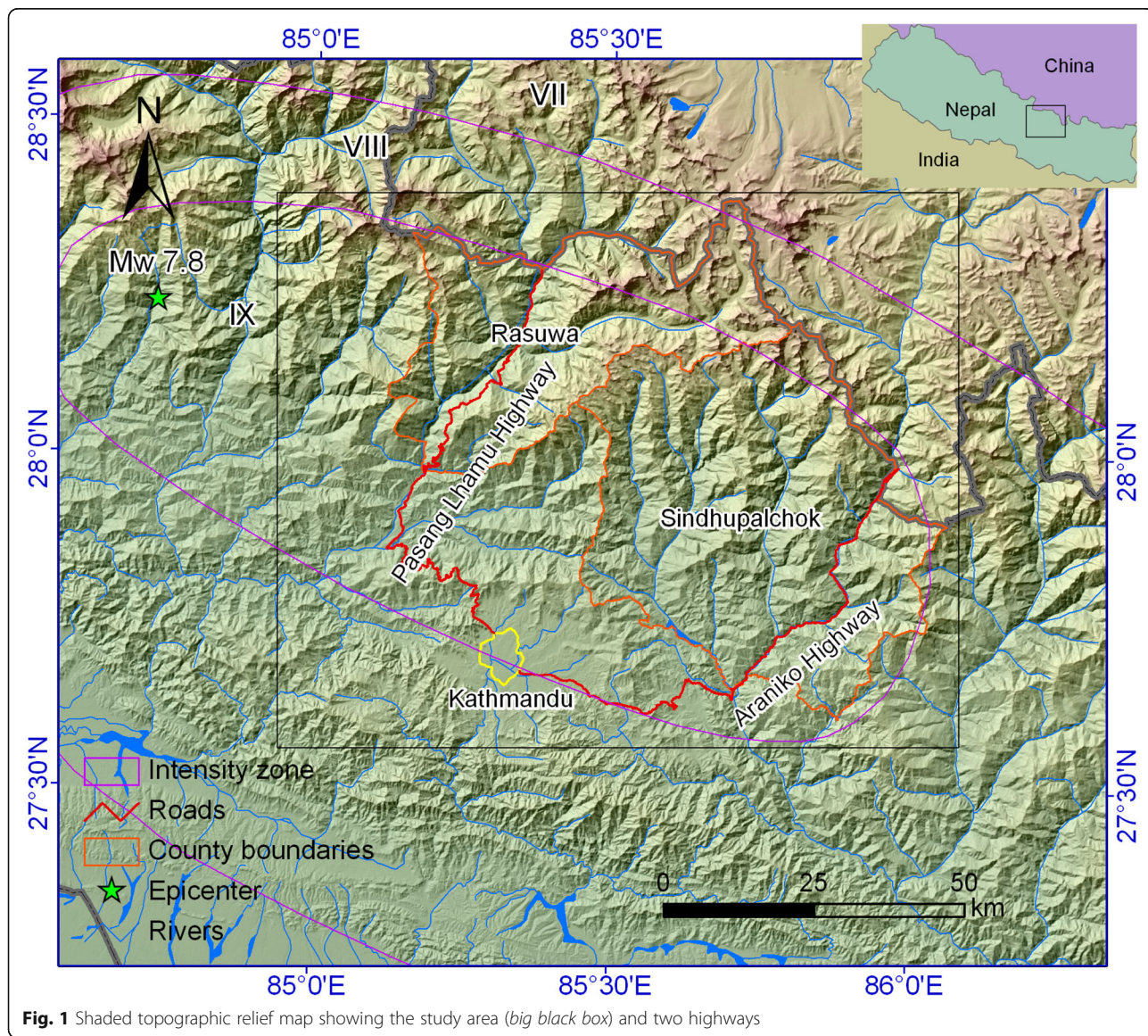


**Fig. 1** Shaded topographic relief map showing the study area (big black box) and two highways

the buffer area of 5 km to the Araniko Highway. Next, correlations between the 3,005 landslides and five landslide controlling factors were analyzed. Finally, we performed landslide hazard assessment for a larger area affected by the Gorkha earthquake using the weigh index (WI) method.

**Data and methods**

**The study area**

Despite its large magnitude, the Gorkha earthquake did not produce visible ruptures on the surface, which was confined to the subsurface at depths 10–15 km (Angster et al. 2015;

Avouac et al. 2015; Hashash et al. 2015; Parameswaran et al. 2015; Duputel et al. 2016; Elliott et al. 2016). The earthquake-affected area is mainly in the east to the epicenter (28.23°N, 84.731°E), likely associated with the eastward rupturing directivity (Wang and Fialko 2015; Koketsu et al. 2016), from which we selected is a rectangular area as the study area, which has a length of 113 km in east-west direction and width of 92 km in north-south direction (Fig. 1), covering 10,396 km<sup>2</sup>. From north to south, the elevation of the study area generally declines from 7,975 m to 387 m, i.e. more than 7,500 m elevation drop in an about 100 km-wide zone. The

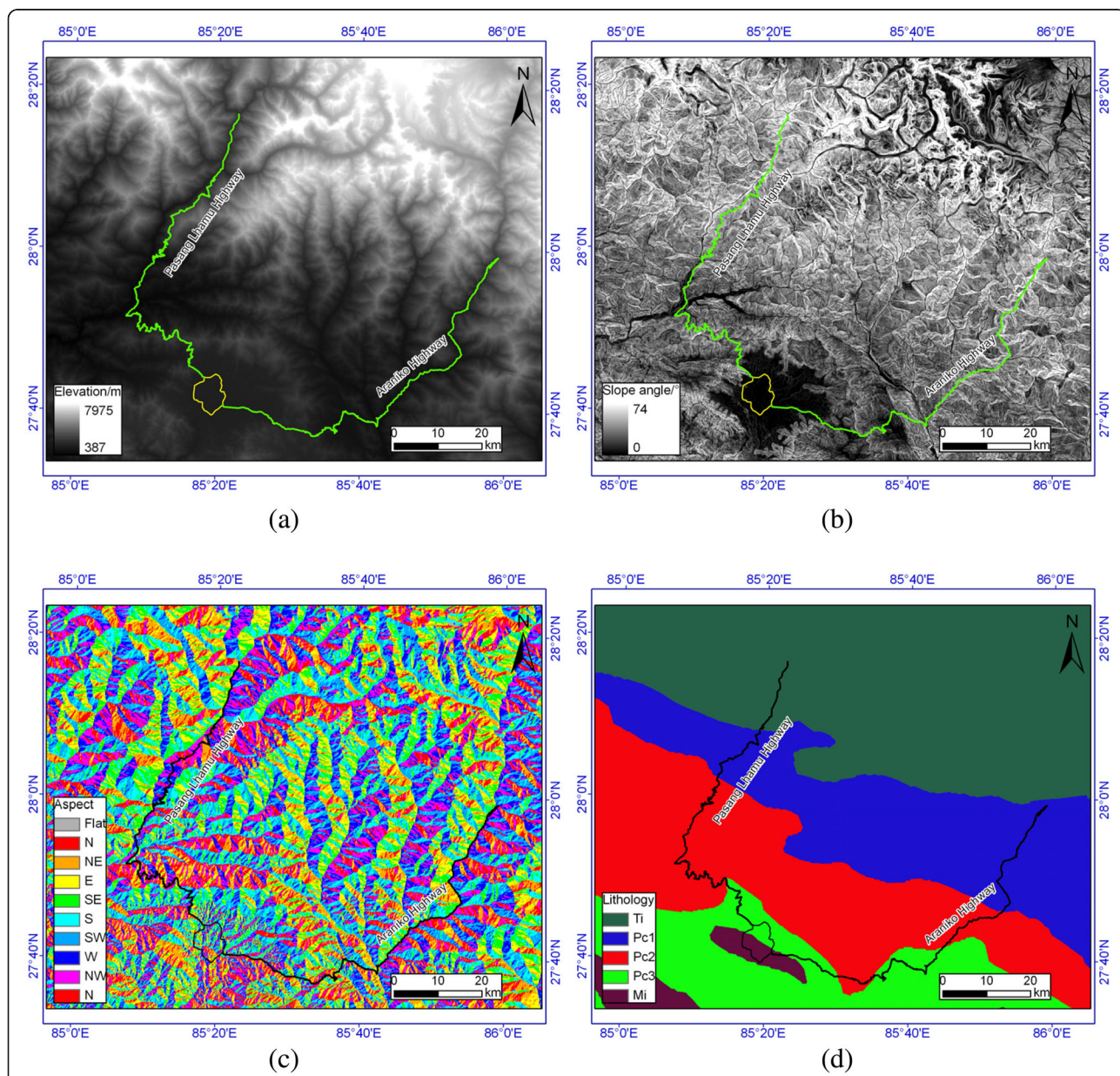


**Fig. 2** Maps showing controlling factors of coseismic landslides of the study area. **a** Elevation. **b** Slope angle. **c** Aspect. **d** Lithology (sources are mentioned in the text)

area encompasses the Rasuwa and Sindhupalchok counties of Nepal (Fig. 1). The Araniko Highway passes through Sindhupalchok county and the Pasang Lhamu Highway passes through Rasuwa county, respectively. Based on the seismic intensity map released by the China Earthquake Administration ([www.cea.gov.cn](http://www.cea.gov.cn)), most of the study area lies in the IX intensity zone, and part in VIII and VII intensity zones (Fig. 1).

**Data**

The satellite images for landslide interpretation are from the Google Earth (GE) platform. After the earthquake occurred, several organizations have implemented specialized tasks to obtain post-earthquake satellite images. Some of the images with very high resolution (1 m or better) are available on the Google Earth platform. In addition, pre-earthquake images with high quality and resolution in the area are also available on the GE platform. These images allow researchers to map co-seismic landslides conveniently and accurately. The regional DEM for analyzing correlations between topography and coseismic landslides were derived from SRTM DEM in 3-arc-second resolution (Fig. 2a). The slope angle map (Fig. 2b) and aspect map (Fig. 2c) were derived from the regional DEM on the GIS platform. The geologic map (Fig. 2d) of the study area was clipped and revised from “World Geologic Maps” on the USGS Website ([www.usgs.gov](http://www.usgs.gov)).

**Methods**

**Landslide identification**

In this study, we used two methods to identify landslides, i.e. visual interpretation of pre- and post-earthquake satellite images and field investigation. Computer screen-based visual interpretation of satellite images is the most widely used method for earthquake-triggered landslide mapping which permits to prepare

high-quality landslide inventories (Xu 2015). As a supplement and verification of results from visual interpretation, we carried out several days of field investigation mainly along the Pasang Lhamu Highway and Araniko Highway.

**Spatial distribution and hazard assessment of landslides**

The Gorkha, Nepal earthquake affected a very large area about tens of thousands of square kilometers. Immediately after the quake, it was difficult to construct a detailed and complete landslide inventory throughout the affected area. Fortunately, spatial distribution of the partial affected area can represent the overall spatial patterns of landslides under some conditions (Lee et al. 2008; Xu et al. 2013a). Therefore, we selected a 5-km buffer area on either side of the Araniko Highway to construct a detailed landslide inventory. Although we prepared a polygon-based inventory of landslides that directly damaged Araniko Highway and Pasang Lhamu Highway, we chose point-based inventory of coseismic landslides and landslide number density (LND, defined as the number of landslides per square kilometers (Xu et al. 2013b) to conduct analysis of the spatial distribution and hazard assessment of landslides. The reasons include: (1) The precise source area of a landslide is very difficult to be distinguished from the whole landslide area because the boundaries of the source area, movement area, and accumulation area of the landslide are usually in the subsurface, thus cannot be exactly delineated, which perhaps reduce the objectiveness of landslides hazard assessment. (2) Preparation of a point-based landslide inventory is relatively time-saving, permitting to carry out a quick regional assessment of earthquake-triggered landslides. Five controlling factors, including elevation, slope angle, slope aspect, lithology, and seismic intensity were taken into account for a statistical analysis. Currently, many statistical methods are available for landslide hazard assessment (Xu et al. 2012; Feng et al. 2016; Pathak 2016; Tsangaratos and Ilia 2016), among which the

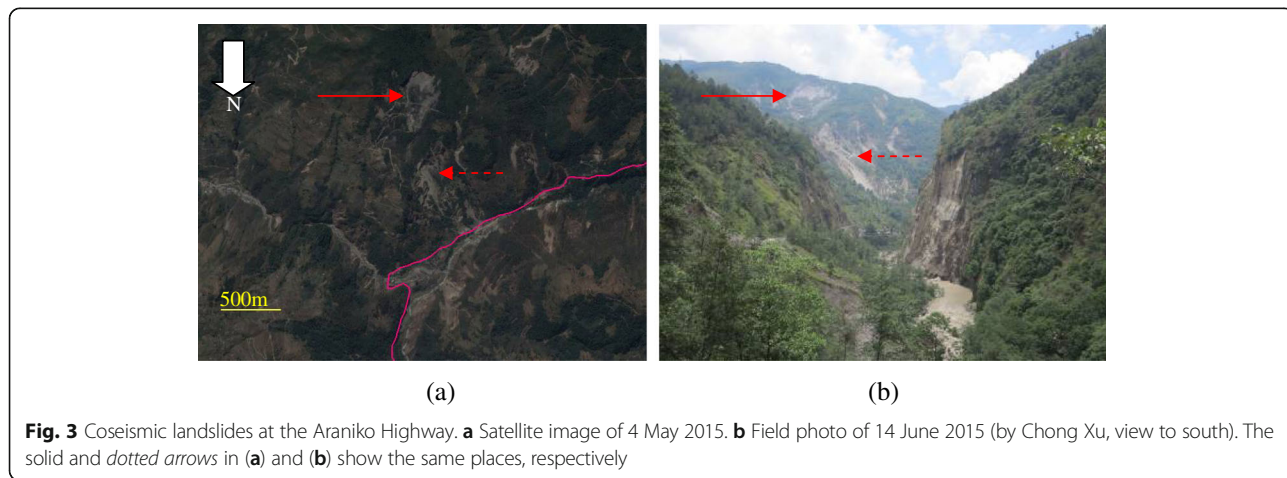




**Fig. 4** Rockfalls on the upper slope of an inspection station of Nepal. **a** Satellite image of 4 May 2015. **b** Field photo of 14 June 2015 (by Chong Xu, view to northwest). The solid and dotted arrows in (a) and (b) indicate the same places, respectively

bivariate statistical analysis method has been widely used in various areas because it is time-saving and does not need complex calculations (Xu et al. 2013b). In this study, a weight index (WI) model was employed to perform landslide susceptibility mapping in the 5-km buffer area aforementioned. This WI method is based on a bivariate statistical analysis based on calculating landslide number density (LND). In this method, the weigh value of each factor class is defined as the natural logarithm of the LND in the class divided by the LND of the whole area (Sarkar et al. 2008; Yalcin 2008; Xu et al. 2013b):

$$\begin{aligned}
 WI_i &= \ln(LND_i/LND) \\
 &= \ln((LN_i/Area_i)/(LN/Area))
 \end{aligned}
 \tag{1}$$

where  $WI_i$  is the weight of the factor-class  $i$ ,  $LND_i$  is the landslide number intensity within the area of the  $i$ th factor class, and  $LND$  is the landslide number intensity in the whole area. In this study, the value of  $LND$  is  $3,005/1,027.4 \text{ km}^2 = 2.925 \text{ km}^{-2}$ .

### Findings, results and analysis

#### Landslides on satellite images

In this section, we present several groups of comparisons of satellite images and field photos of coseismic landslides to illustrate the excellent capacity of detecting coseismic landslides on high-resolution satellite images. The satellite images used in this study are from the GE platform collected in early May, 2015. The red solid arrow on Fig. 3 shows a coherent landslide (27.87°N, 85.911°E) with clear exposed bedrocks in the landslide source area and partly damaged vegetation stayed at its deposit area. The red dotted line defines several shallow, disrupted landslides along the Araniko Highway road. Due to the high resolution and quality of the satellite image, the locations and boundaries of the landslides can be mapped correctly and conveniently on the ortho images.

Figure 4 shows two rockfalls (27.927°N, 85.932°E) occurred on the upper slope at an inspection station of Nepal, which originated from nearby the ridge of the reverse slope and accumulated into two conical heaps with two narrow runout paths. The broken accumulate



**Fig. 5** A series of shallow, disrupted landslides blocking the Pasang Lhamu Highway. **a** Satellite image of 3 May 2015. **b** Field photo of 15 June 2015 (by Chong Xu, view to southeast) showing the road was blocked by a secondary landslide caused by a heavy rainfall. The red solid arrow in (a) shows the location of field photo in (b)



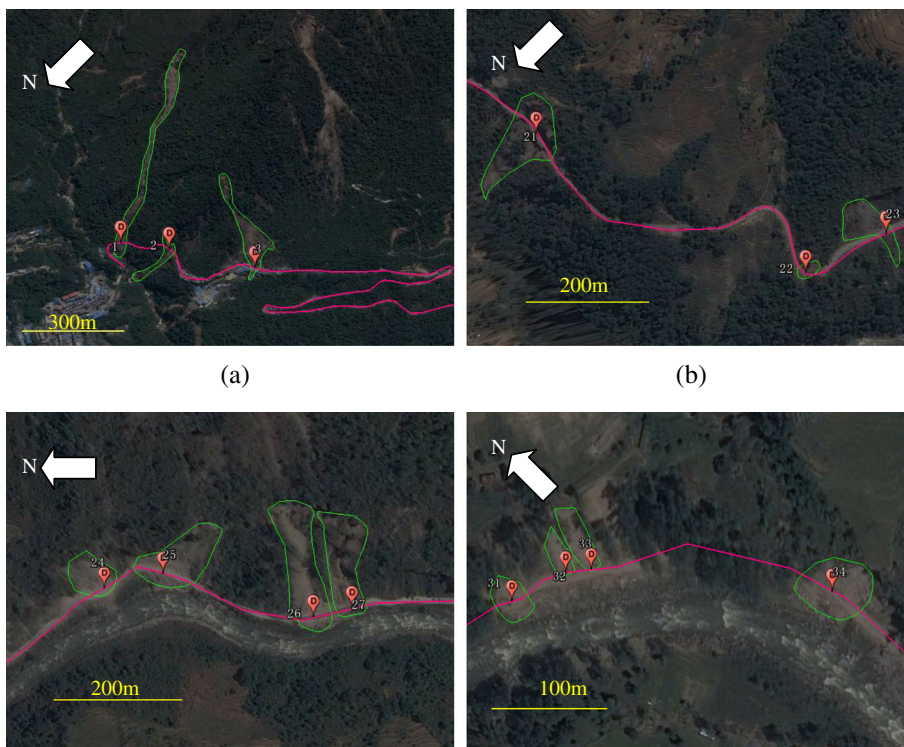
(a) (b)

**Fig. 6** An area characterized by high density of coseismic landslides. **a** Satellite image taken on 3 May 2015. **b** Field photo taken on 15 June 2015 (by Chong Xu, view to west). The solid and dotted arrows denote the same places, respectively

materials are dangerous for the structures on the toe of the slope. Despite different expressions of the rockfalls on the image and field photos due to the image stretching caused by steep topography, the rockfalls can be easily identified on the satellite image with the aid of field investigations. They have short runout distances on the image, whereas the actual runout distances of them are likely longer. This is because the slope of the rockfalls occurrence is

almost vertical. Small rockfalls or falling stones are more susceptible than large deep-seated landslides on such a reverse slope.

After the main shock, a series of aftershocks and rain-falls struck the affected area and caused more landslides. For example, the satellite image of 3 May 2015 (Fig. 5a) shows quite a few shallow, disrupted landslides (located at 28.064°N, 85.225°W) that occurred in weathering layers



(a) (b) (c) (d)

**Fig. 7** Damaged sites along Araniko Highway by coseismic landslides have been seen on satellite images. The detailed information of the landslides and associated damages on the road is listed in Table 1. **a** the No. 1, 2, and 3 landslides, **(b)** the No. 21, 22, and 23 landslides, **(c)** the No. 24, 25, 26, and 27 landslides, and **(d)** the No. 31, 32, 33, and 34 landslides along Araniko Highway. All the satellite images were acquired on 4 May, 2015

and blocked the Pasang Lhamu Highway. Fig. 5b shows the road was blocked by a secondary landslide caused by a heavy rainfall in the area. Information from local residents suggests that the landslide accumulation material that blocked the road was not triggered by the main shock, but by a strong rainfall a few days before. All the landslide

materials related to the main shock and subsequent triggers blocking the roads have been cleared up or were being cleared away in time to keep the traffic flowing.

The satellite image (Fig. 6a) shows an area with high density of coseismic landslides, dominated by shallow, disrupted landslides. The red solid arrows wherein

**Table 1** Information of damage along the Araniko Highway and associated coseismic landslides

No.	Longitude (°)	Latitude (°)	Length of road damaged (m)	Area (m <sup>2</sup> )	Estimated volume (m <sup>3</sup> )
1	85.98343	27.9868	45	29131	50000
2	85.98196	27.98562	52	6180	12000
3	85.9791	27.98369	35	22953	60000
4	85.96235	27.97215	16	3648	6000
5	85.96186	27.97166	27	3756	7000
6	85.96482	27.96926	29	8383	20000
7	85.96511	27.96912	30	ditto	ditto
8	85.95799	27.96591	10	435	400
9	85.93064	27.91744	156	31816	20000
10	85.92627	27.91352	19	4233	8000
11	85.9227	27.90877	5	972	1000
12	85.92241	27.90828	27	2271	3000
13	85.9222	27.9079	33	2630	4000
14	85.91496	27.8927	10	15890	30000
15	85.91307	27.88253	30	1739	2000
16	85.90599	27.87934	46	12025	30000
17	85.90493	27.87892	12	268	200
18	85.90185	27.87782	115	6224	10000
19	85.89957	27.87686	49	4245	6000
20	85.89595	27.87602	15	303	200
21	85.88781	27.87385	95	9237	20000
22	85.88341	27.87226	25	608	500
23	85.88309	27.87113	20	3583	5000
24	85.88062	27.85115	43	3805	5000
25	85.88092	27.85034	94	7461	15000
26	85.88045	27.84828	54	9367	20000
27	85.88063	27.84779	42	7061	15000
28	85.87291	27.82729	57	3399	5000
29	85.87352	27.82707	43	3094	5000
30	85.89329	27.8036	15	1250	1500
31	85.89425	27.80022	30	949	1000
32	85.89475	27.80006	13	522	300
33	85.89492	27.79994	7	937	1000
34	85.89613	27.7986	52	1971	2500
35	85.88417	27.77117	1	628	500
36	85.77906	27.73006	63	3778	5000
Total			1,415	214,751	372,100

No. 6 and No. 7 landslide-damaged sections were caused by one landslide

**Table 2** Information of damaged along the Pasang Lhamu Highway and associated coseismic landslides

No.	Longitude (°)	Latitude (°)	Length of road damaged (m)	Area (m <sup>2</sup> )	Estimated volume (m <sup>3</sup> )
1	85.24384	27.82563	12	166	100
2	85.23569	27.82943	14	613	500
3	85.20104	27.83575	14	275	200
4	85.13849	27.8637	17	628	500
5	85.18591	27.98131	18	311	200
6	85.1884	27.98278	14	197	100
7	85.18866	27.98288	16	209	100
8	85.18777	27.9828	50	1144	1200
9	85.21029	28.00465	16	336	300
10	85.2181	28.01873	9	177	100
11	85.22025	28.02089	21	553	400
12	85.22087	28.02175	28	2766	4000
13	85.22311	28.02457	40	32568	80000
14	85.22349	28.02528	48	17673	50000
15	85.22334	28.02617	39	10247	20000
16	85.22309	28.02716	45	9266	20000
17	85.22299	28.02766	18	10071	20000
18	85.21933	28.0394	14	199	100
19	85.22441	28.04657	14	227	100
20	85.22547	28.04732	7	171	100
21	85.22722	28.04826	24	805	800
22	85.22892	28.05021	22	279	200
23	85.22869	28.05054	14	103	100
24	85.22923	28.05373	5	271	200
25	85.22867	28.05858	19	11564	5000
26	85.22811	28.06002	53	3790	5000
27	85.22798	28.061	67	7609	15000
28	85.22674	28.0633	57	5222	10000
29	85.22643	28.06371	19	1815	2000
30	85.22562	28.0644	28	9168	20000
31	85.22542	28.06454	15	3018	4000
32	85.22515	28.06481	14	525	300
33	85.22494	28.06501	21	2679	3000
34	85.22447	28.06545	31	5012	5000
35	85.22374	28.06637	36	3662	5000
36	85.22535	28.06689	25	2876	4000
37	85.22884	28.06806	59	11267	20000
38	85.23007	28.06827	99	20358	60000
39	85.23904	28.07238	209	54607	200000
40	85.25552	28.0772	16	920	800
41	85.2558	28.07737	11	152	100
42	85.25023	28.07813	13	500	300
43	85.277	28.09335	18	241	100

**Table 2** Information of damaged along the Pasang Lhamu Highway and associated coseismic landslides (Continued)

44	85.27853	28.09454	15	169	100
45	85.2867	28.10178	9	95	100
46	85.28784	28.104	7	109	40000
47	85.2877	28.10459	104	15961	3000
48	85.28754	28.1055	30	2082	3000
49	85.28715	28.10675	14	577	500
50	85.31217	28.10857	19	1711	2000
51	85.31202	28.10873	22	1306	1500
52	85.31183	28.11008	60	10024	250000
53	85.31135	28.11061	49	4482	8000
54	85.31117	28.11098	17	1550	2000
55	85.29239	28.11159	24	555	500
56	85.31072	28.11175	41	3888	6000
57	85.31043	28.11217	55	7463	15000
58	85.29454	28.11298	6	168	100
59	85.30909	28.11914	11	117	100
60	85.30815	28.12234	14	5918	12000
61	85.30685	28.12406	4	357	300
62	85.34242	28.17233	25	957	1000
63	85.34248	28.17269	31	4223	8000
64	85.34254	28.17314	14	1996	2000
65	85.3426	28.17358	63	21402	60000
66	85.34237	28.178	18	1374	2000
67	85.34225	28.17896	11	695	800
68	85.3439	28.18229	14	197	100
69	85.34455	28.18387	17	4005	6000
70	85.34617	28.18621	30	33718	100000
71	85.34634	28.18678	57	32800	100000
72	85.34741	28.18903	16	565	500
73	85.34761	28.18932	24	8214	10000
74	85.34883	28.19127	59	18536	30000
75	85.34972	28.19332	14	445	300
76	85.35092	28.19643	19	398	300
77	85.35147	28.19703	41	4677	80000
78	85.35182	28.19742	27	3538	5000
79	85.35224	28.19803	13	1716	1000
80	85.35285	28.19931	19	3032	3000
81	85.35292	28.19967	12	1805	1000
82	85.35304	28.20057	43	2852	5000
83	85.35425	28.20403	41	1693	2500
84	85.35507	28.20837	38	4976	10000
85	85.35804	28.2197	102	13969	40000
86	85.36041	28.22164	19	3995	5000
87	85.36106	28.22261	107	14279	30000



**Table 2** Information of damaged along the Pasang Lhamu Highway and associated coseismic landslides (*Continued*)

88	85.36698	28.25649	44	2549	4000
89	85.37802	28.27514	92	21169	60000
Total			2,842	500,552	1,470,600

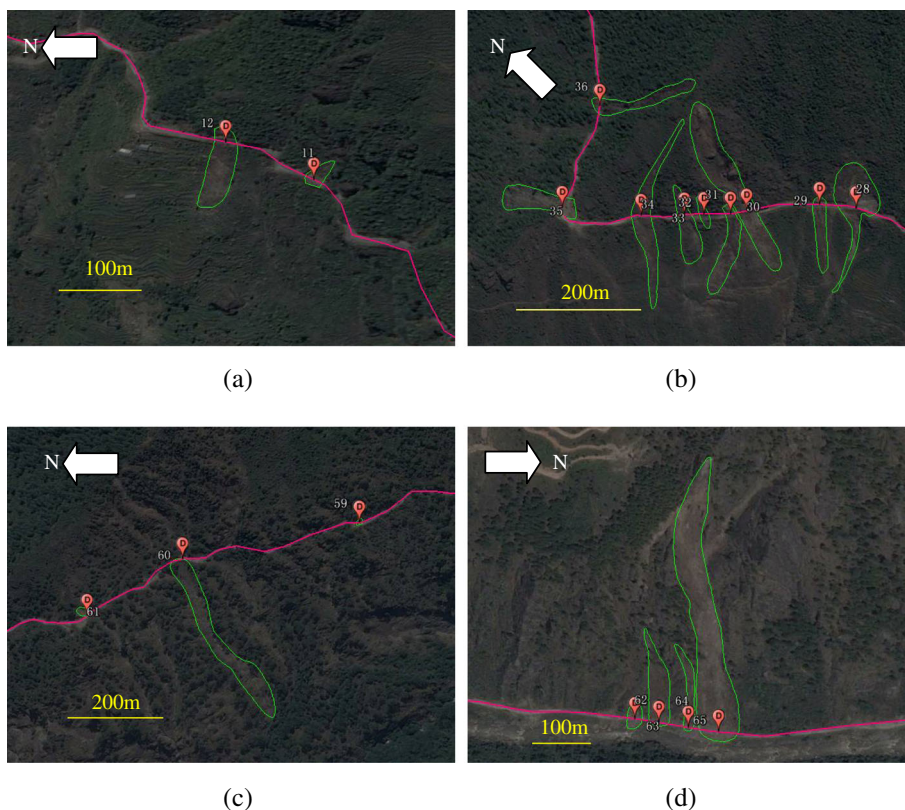
indicate a large rock slide located at 28.079°N, 85.194°W. It occurred at the lower part of the slope and blocked the valley. However, they did not create a lake because of the small area of the catchment upstream. The red dotted arrows show a shallow, disrupted landslide originated from a ridge (located at 28.08°N, 85.208°W). Most of the landslides shown in Fig. 6a are distributed along the rivers, likely associated with river incision or loose deluvium with high landslide susceptibility.

**Landslide damage to the two roads**

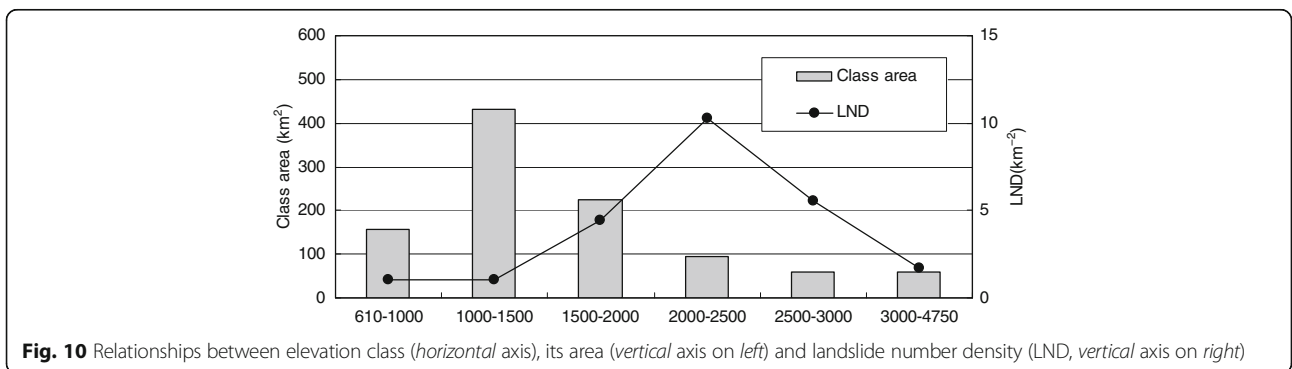
The Pasang Lhamu Highway and Araniko Highway are two most important roads connecting Nepal and China. The Araniko Highway links Kathmandu, Nepal and Nielamu County, China. In this study, the section of the Araniko Highway between the place (27.987262°N, 85.982552°E) nearby Zhangmu Port and the location

(27.678835°N, 85.349647°E) southeast to Kathmandu was selected as the target to investigate the damage of coseismic landslides on the road. This section of Araniko Highway is about 117.3 km long. Based on visual interpretation of high-resolution satellite images and field investigations, we delineated 35 coseismic landslides damaging the Araniko Highway at 36 places. The longest section of the road damaged is about 156 m long which was buried by a landslide at 27.91744°N, 85.93064°E. Considering the previous correlations between area and volume of individual landslides (Larsen et al. 2010; Xu et al. 2016b) and field investigations, the total volume of the 35 coseismic landslides was estimated to be about 0.37 million m<sup>3</sup>. Figure 7 shows the Araniko Highway damaged by coseismic landslides on satellite images at four places. Table 1 lists the detailed information on the 35 coseismic landslides and hazards on the road they caused.

The Pasang Lhamu Highway connects Kathmandu, Nepal and Gyirong County. The length of the section between the point (27.735268°N, 85.305939°E) northwest to Kathmandu and the point (28.278972°N, 85.377904°E) China-Nepal border is about 139.3 km. Visual interpretation of satellite images and field investigations allowed us to delineate 89 coseismic landslides that damaged the



**Fig. 8** Damaged sites along Pasang Lhamu Highway by coseismic landslides on satellite images. The detailed information of the landslides and associated damages on the road is listed in Table 2. **a** the No. 11 and 12 landslides, **(b)** the No. 28–36 landslides, **(c)** the No. 59, 60, and 61 landslides, **(d)** the No. 62, 63, 64, and 65 landslides along Pasang Lhamu Highway. All the satellite images were acquired on 3 May, 2015



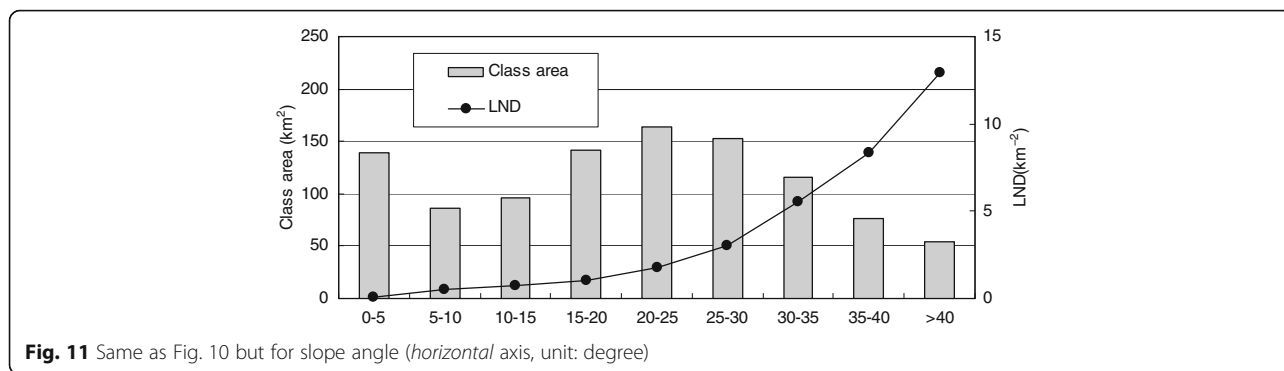


**Fig. 11** Same as Fig. 10 but for slope angle (*horizontal axis, unit: degree*)

Pasang Lhamu Highway. The total length of damaged or buried roads is about 2,842 m, of which the longest section is about 209 m long, caused by a landslide located at 27.91744°N, 85.93064°E. The total volume of the 89 landslides was estimated to be 1.47 million m<sup>3</sup>. Figure 8 shows satellite images of coseismic landslides along the Pasang Lhamu Highway. Table 2 shows the detailed information on the 89 coseismic landslides and their hazards on the road.

**Landslide inventory along the Araniko highway**

On either side of the 117.3 km-long Araniko Highway, we constructed a 5-km buffer region to construct a detailed and complete point-based coseismic landslide inventory. The area of this buffer region is 1,027.4 km<sup>2</sup>. Individual coseismic landslides were mapped as points at the central of the landslide. Consequently, we mapped 3,005 coseismic landslides in the area (Fig. 9), and calculated the landslide number density to be 3,005/1,027.4 km<sup>2</sup> = 2.925 km<sup>-2</sup>. The spatial distribution of the coseismic landslides along the Araniko Highway is quite uneven. Most of the landslides occurred in the mountainous areas to the north, where the landslide inventory is complete and detailed, i.e. small landslides are included. The buffer area only accounts for less 10% than the primary affected area of the main shock. The buffer area is approximately normal to the strike of the seismogenic structure (EW trending). Usually the seismic landslide density along the causative fault is uniform.

Therefore, we estimated the Gorkha quake triggered at least 30,000 landslides. Several other teams have released coseismic landslides related to the Gorkha quake. For example, Kargel (Kargel et al. 2016) only mapped 4,312 coseismic and postseismic landslides. A team from British Geological Survey et al. (British Geological Survey et al. 2015) identified about 5,600 coseismic landslides as polylines marking the location and movement path from head to toe of a landslide. Therefore, there might be false negative errors (omissions) in these released inventories of landslides triggered by the Gorkha quake.

**Spatial distribution of landslides along the Araniko highway**

As a common index to reflect landslide abundance, landslide number density was employed as the index to measure spatial distribution of the 3,005 landslides in the 5-km buffer area of the Araniko Highway. In this study, five controlling factors including elevation, slope angle, slope aspect, lithology, and seismic intensity were selected to analyze their correlations with the landslides (Figs. 10, 11, 12, 13 and 14). The DEM of the area was derived from SRTM in 3 arc-second, which permitted to determine the elevations of the buffer area vary from 610 m to 4,750 m. The study area was divided into six classes based on 500 m of elevation intervals, i.e. 610–1000 m, 1000–1500 m, 1500–2000 m, 2000–2500 m, 2500–3000 m, and 3000–4750 m (Fig. 10). The

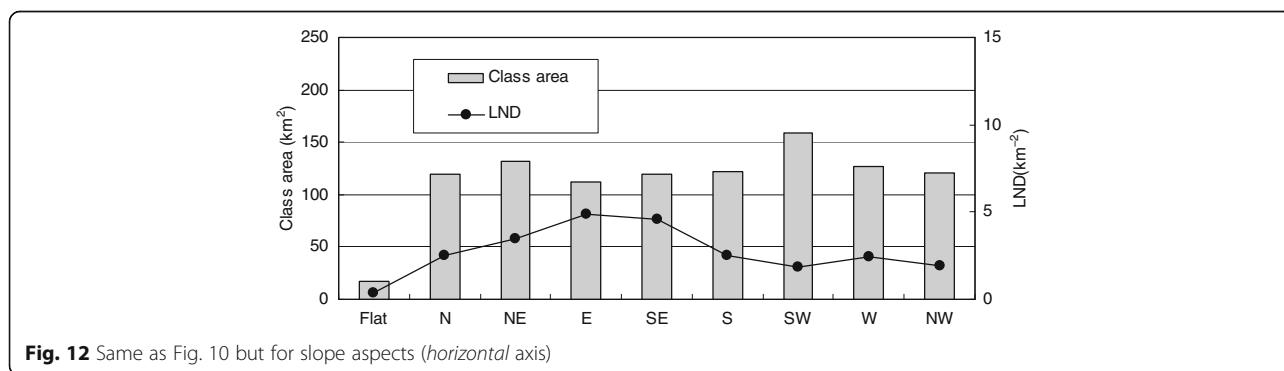


**Fig. 12** Same as Fig. 10 but for slope aspects (*horizontal axis*)

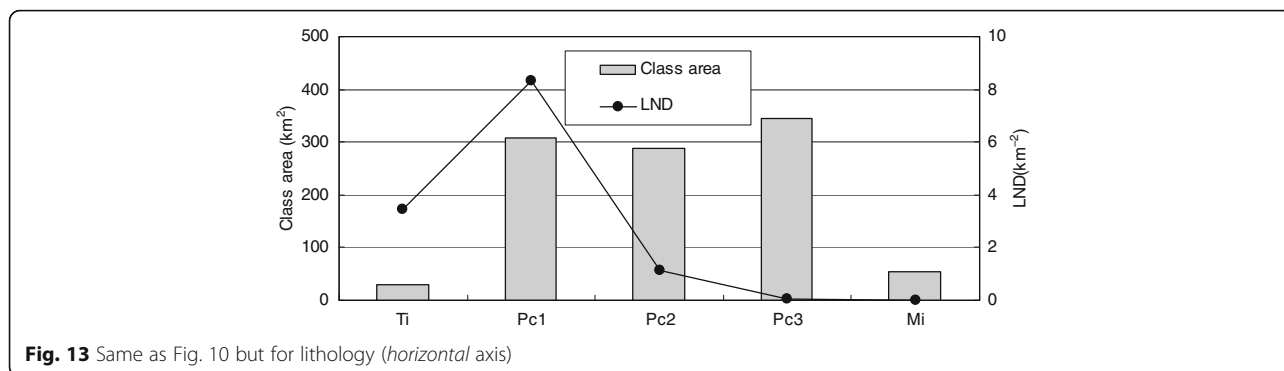


**Fig. 13** Same as Fig. 10 but for lithology (horizontal axis)

elevations of most of the area (814.97 km<sup>2</sup>, 79.3% of the total) are lower than 2,000 m. The class 1000–1500 m occupies the largest area, which is 433 km<sup>2</sup>, accounting for 42.1% of the total. The class 2,000–2,500 m registered the largest LND value, which is 10.3 km<sup>-2</sup>. The landslide number density values gradually decrease at the elevations higher than 2,500 m and lower than 2,000 m.

Slope angle is an important controlling factor of coseismic landslides. In this study, the slope angle of the buffer area ranges from 0° to 74°, which was divided into 9 classes with an interval of 5°. Majority of the area (780.7 km<sup>2</sup>, 76% of the total) has slope angles lower than 30°. As shown in Fig. 11, the landslide number density increases with the growing slope angle. The class >40° corresponds to the largest LND value, which is 12.92 km<sup>-2</sup>. In addition, the LND curve shows a concave form, implying the LND increases with the slope angle gradually. This suggests a very strong control of the slope angle on the coseismic landslides. Such a situation is also common in other earthquake events (Gorum et al. 2014; Xu et al. 2014; Xu et al. 2015; Tian et al. 2016).

Slope aspects (or facing directions) can affect the pattern of coseismic landslides because slopes with different aspects have varied responses to the movement directions of blocks or the propagating direction of seismic waves. The study area has nine classes of slope aspects, i.e. flat, north (N), northeast (NE), east (E), southeast (SE), south (S), southwest (SW), west (W), and

northwest (NW). Fig. 12 shows the correlations between the slope aspect, area of its classes and landslide number density. It is clear that the slope aspects E and SE correspond to the two largest LND values, which are 4.87 km<sup>-2</sup> and 4.58 km<sup>-2</sup>, respectively. This is perhaps related to the movement direction of the hanging wall of the seismogenic fault or the propagation direction of seismic wave (Shen et al. 2016). The study area is located east of the epicenter of the Gorkha main shock, and thus the propagating direction of seismic waves is eastward. During the Gorkha earthquake, the hanging wall of the fault, where the buffer area is located, moved toward south and probably generated inertia effect to the south. In addition, the slopes of southward aspect in the area are easily exposed to sunlight and rainfall, thus leading to widespread weathering layers and high susceptibility to seismic landslides.

The Gorkha earthquake affected area can be divided into a series of east-west trending major tectonic regions by three major active fault zones, including MFT, MBT, and MCT (Le Fort 1975; Nakata 1989; Upreti 1999; Wesnousky et al. 1999; Mukherjee 2015). Based on the geologic map of South Asia, the study area has five classes of lithology (rock types) generally from north to south, i.e. Tertiary igneous rocks (Ti), Precambrian rocks-1 (Pc1), Precambrian rocks-2 (Pc2), Precambrian rocks-3 (Pc3), and Mesozoic intrusive rocks (Mi). Figure 13 shows the correlations between lithology, its

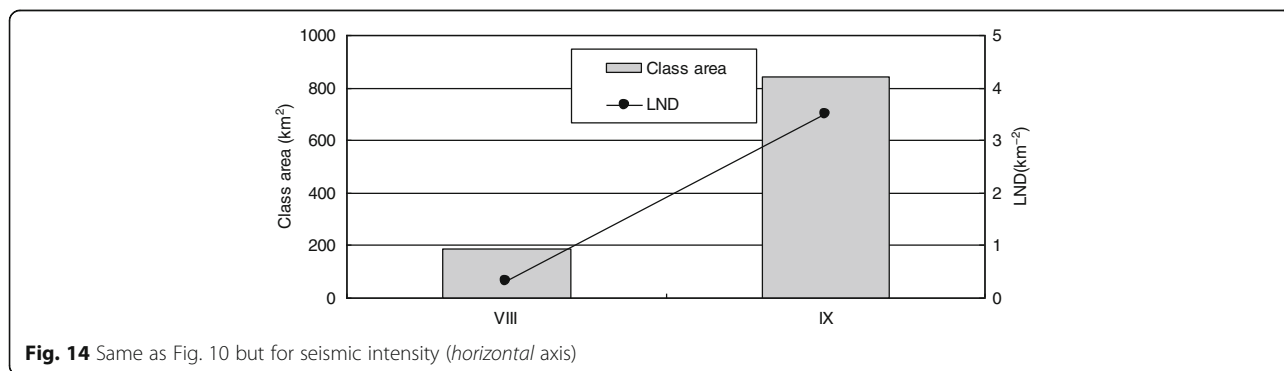


**Fig. 14** Same as Fig. 10 but for seismic intensity (horizontal axis)

class area and landslide number density. The three groups of Precambrian rocks cover most of the area, which is 942.8 km<sup>2</sup>, occupying 91.8% of the total. The lithology class Pc1 registered the largest landslide number density, which is 8.32 km<sup>-2</sup>.

Seismic intensity and peak ground accumulation (PGA) are two common proxies representing the degree of seismic energy and often used to explore the effect of earthquakes on landslides. The PGA distribution map released by USGS ([www.usgs.gov](http://www.usgs.gov)) is rather irregular in the 5-km buffer area of the Araniko Highway because the buffer area is relatively small and there are perhaps significant errors generated by numerical simulation and limited stations. Therefore, we preferred to analyze the correlation between coseismic landslides and seismic intensity in this study. The seismic intensity map of the Gorkha earthquake was produced by China Earthquake Administration (CEA) (Fig. 1). Only VIII and IX intensity zones appear in the study area, which have the landslide number density values 0.32 km<sup>-2</sup> and 3.5 km<sup>-2</sup>, respectively (Fig. 14). Despite merely two data points, these data show a positive correlation with the coseismic landslides, i.e. the place with larger seismic intensity has a higher landslide number density.

**Landslide hazard assessment**

In the aforementioned 5-km buffer area of the Araniko Highway, the WI vales were calculated to each class of all the five controlling factors, respectively. Then, the weighted thematic maps of the five factors were produced and were superposed to derive a landslide hazard index (LHI) map:

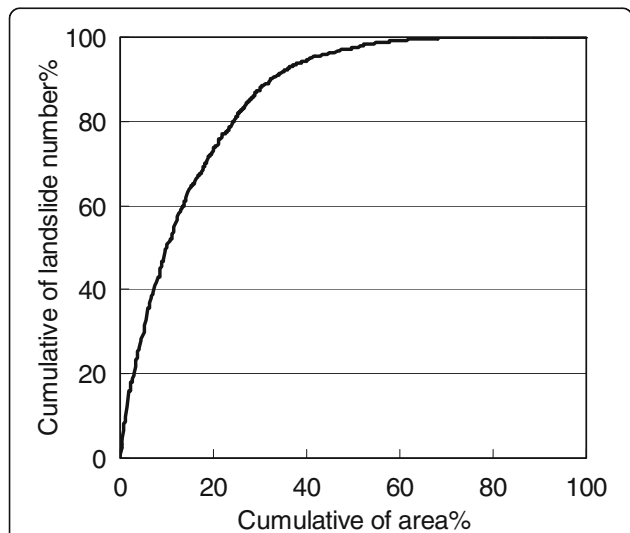


**Fig. 15** The area under the curve representing the success ratio of the landslide hazard assessment. Area % means the percentage of area to the study area for each factor class. Landslide number % means the percentage of landslide number in a factor class to the total landslide number

$$LHI = WI_{Elevation} + WI_{Slope\ angle} + WI_{Slope\ aspect} + WI_{Lithology} + WI_{Seismic\ intensity} \quad (2)$$

The WI values indicate the relative importance of each factor to landslide hazard. Positive WI values mean the factor-class area is prone to coseismic landslides,

**Table 3** Weight index values of various classes of five controlling factors

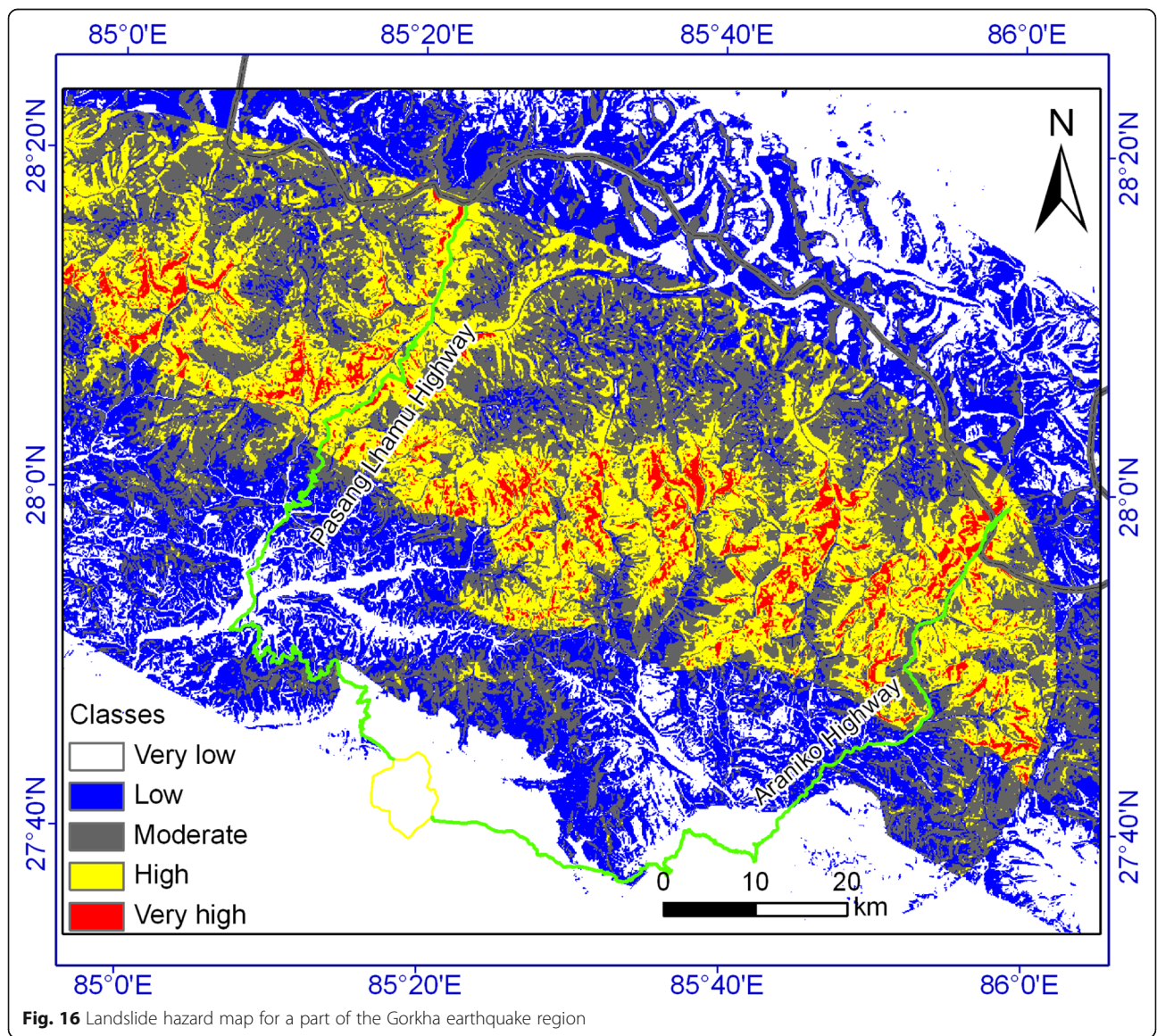
Factor	Class area	Landslide number	LND	WI
<b>Elevation</b>				
610–1000 m	155.94	159	1.02	-1.05
1000–1500 m	433	438	1.01	-1.06
1500–2000 m	226.03	1000	4.42	0.41
2000–2500 m	95.24	981	10.3	1.26
2500–3000 m	58.83	327	5.56	0.64
3000–4750 m	58.39	100	1.71	-0.54
<b>Slope angle</b>				
0–5°	139.07	15	0.11	-3.3
5–10°	86.75	42	0.48	-1.8
10–15°	96.61	71	0.73	-1.38
15–20°	141.86	144	1.02	-1.06
20–25°	163.49	290	1.77	-0.5
25–30°	152.92	458	3.00	0.02
30–35°	115.59	641	5.55	0.64
35–40°	76.65	640	8.35	1.05
40–74°	54.5	704	12.92	1.49
<b>Slope aspect</b>				
Flat	16.63	6	0.36	-2.09
N	120.07	300	2.50	-0.16
NE	131.27	459	3.50	0.18
E	112.63	549	4.87	0.51
SE	119.02	545	4.58	0.45
S	121.36	305	2.51	-0.15
SW	158.51	295	1.86	-0.45
W	127.22	312	2.45	-0.18
NW	120.72	234	1.94	-0.41
<b>Lithology</b>				
Ti	29.34	101	3.44	0.16
Pc1	308.10	2564	8.32	1.05
Pc2	288.82	324	1.12	-0.96
Pc3	345.91	16	0.05	-4.15
Mi	55.26	0	0	-14.89
<b>Seismic intensity</b>				
VIII	185.60	60	0.32	-2.2
IX	841.84	2945	3.5	0.18

Lithology type Mi registered no landslide. In order to avoid ln(0) in calculating WI value, we assigned the LND value of the class Mi with 0.000001, i.e. a small enough value, and the WI value of the class is -14.89

whereas negative WI values represent the opposite. WI values close to zero mean moderate probabilities of occurrence of coseismic landslides. Results show the LHI of the area is in the range from -23.546 to 4.48. In order to examine the validity of the model, the 3,005 coseismic landslides aforementioned were employed to compare the known landslides with the landslide hazard index map. By referring to a common method, the regional area was categorized into 100 classes with a same area by the LHI value and the percentages of landslide number in each class were calculated. Then, a correlation curve between cumulative area percentages and cumulative percentage of landslide number from high to low LHI in a descending order was drawn (Fig. 15). It shows the area under the curve (AUC) is as much as 85.9%, i.e. a quite satisfactory success ratio. The curve also reveals

that 10% of the area with the highest landslide hazard index could cover 1,514 landslides, about 50.4% of the total. Likewise, 20 and 30% of the area with the highest landslide hazard index can account for 2,207 and 2,645 landslides, about 73.4 and 88% of the total, respectively.

We applied the WI values in Table 3 to a larger area, i.e. the rectangle in Fig. 1, to construct a landslide hazards map. For the areas with factor-attribute values beyond the ranges of the 5-km buffer area, they are classified into the classes that are closest to them. The elevation ranges from 291 m to 7968 m in the area. The area with elevation less than 610 m was classified into the class 610–1000 m and the area with elevation higher than 4,750 m was classified into the class 3000–4750 m. The range of slope angle of the rectangle area is 0–81.7°, therefore, the range of 74°–81.7° was merged into the



class 40–74°. The northern part of the rectangle area outcrop several other lithology types, such as Quaternary perennial ice and snow, Quaternary sediments, Neogene granite, Triassic metamorphic and sedimentary rocks, and Cretaceous sedimentary rocks. The northern rock group located at the northern part of the study area was not subdivided further because of limited geologic information there. The WI values of these lithology types were assigned the values same as the type Tertiary igneous rocks (Ti). The rectangle area includes three seismic intensity zones, i.e. VII, VIII, and IX (Fig. 1). The seismic intensity VII is out of the range of the 5-km buffer area and its WI value was calculated by linear extrapolation, which is -4.58. Subsequently, we constructed the LHI map of the rectangle area. We divided the map into four classes, i.e. very low, low, high, and very high, based on three breakpoints of the index values, i.e. -3, -1, 1, and 3. Figure 16 shows the derived landslide hazard map of the study area. The high zone and very high zone show a NWW-SEE directed distribution, which is coincident with the seismogenic fault and earthquake damage area. Figure 17 shows a three-dimensional view on the landslide hazard map. We overlaid the hazard map with 50% transparency on satellite images of the Google Earth platform. However, several limitations of this result should be noted, including (1) Only five common factors were considered, while there should more factors can affect the occurrence of the coseismic landslides, such as

rivers and seismogenic fault. (2) The weight value method is a bivariate method, interactions among factors cannot be considered; and (3) WI values were calculated based on the 3,005 landslides in the 5-km buffer area along the Araniko Highway. Of course, it is inferior to use of a complete inventory of landslides throughout the earthquake-affected area. These limitations are expected to be improved in future research.

**Conclusions**

Based on high-resolution satellite images, field investigation, and GIS technology, we examined the coseismic landslides of the 2015 Gorkha, Nepal earthquake that blocked or damaged the Araniko Highway (117.3 km) and Pasang Lhamu Highway (139.3 km) in Nepal. Results show 35 coseismic landslides damaged the Araniko Highway with a total length of the sections of the damaged road about 1,415 m. The total volume of these 35 coseismic landslides was estimated to be about 0.37 million m<sup>3</sup>. We delineated 89 coseismic landslides that damaged the Pasang Lhamu Highway. The total length of the damaged or buried roads is about 2,842 m. The total volume of these 89 landslides was estimated to be 1.47 million m<sup>3</sup>. In the 5-km buffer area on either side of the Araniko Highway, we mapped 3,005 landslides caused by the Gorkha earthquake. The landslide number density of the buffer area is 2.925 km<sup>-2</sup>. Correlations between the landslides and five controlling factors were

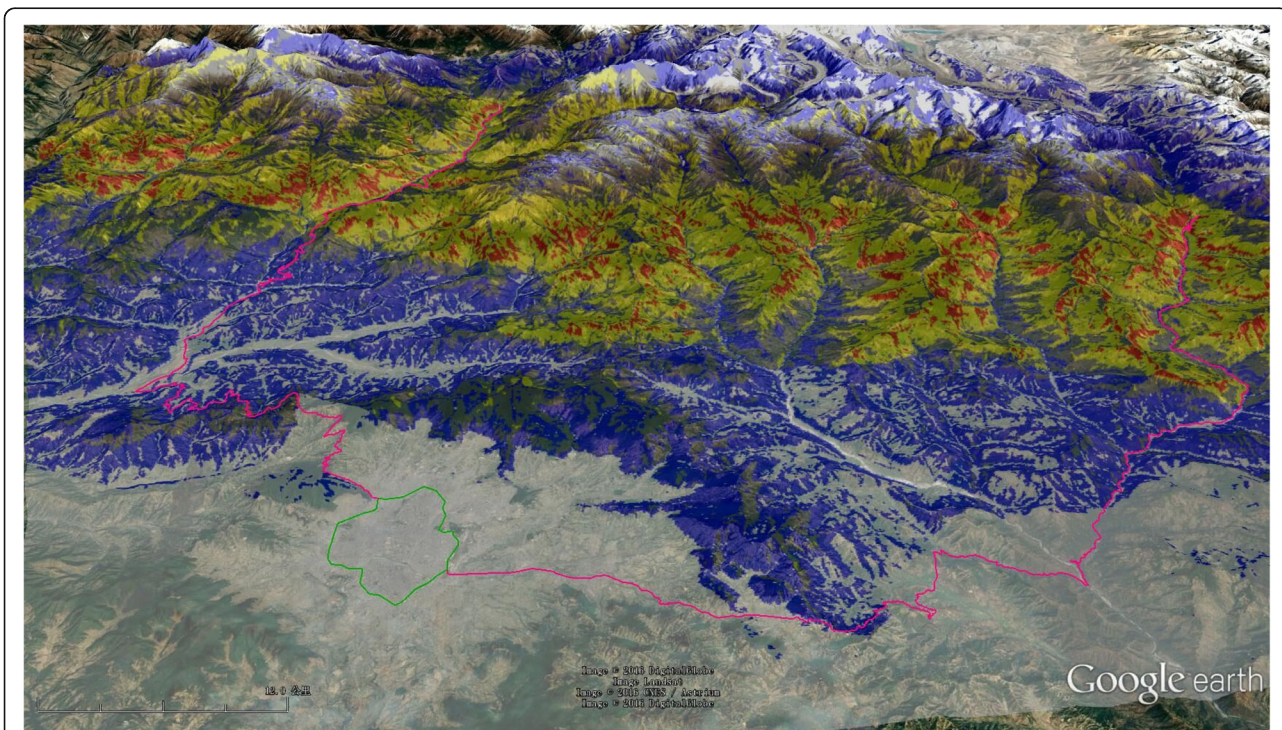


**Fig. 17** A printing screen showing a three-dimensional perspective on the landslide hazard map. View to north

analyzed based on the bivariate method. The results show the elevation class 2,000–2,500 m has the highest landslide concentration. The landslide number density value increases with the slope angle. The slope aspects E and SE correspond to the highest concentrations of coseismic landslides. The underlying bedrock of Precambrian rocks-1 (Pc1) registered the largest landslide number density. The area with seismic intensity IX has a much higher LND value than the area of the intensity VIII. We used the weigh index method to perform landslide hazard assessment in the 5-km buffer area. Result shows the success ratio as high as 85.9%. In addition, we prepared a landslide hazard assessment map for a larger area encompassing Rasuwa and Sindhupalchok counties of Nepal. It indicates the areas most likely to be prone to coseismic landslides, which would be helpful for constructing a more detailed and complete coseismic landslide inventory map throughout the earthquake-affected area subsequently. The result is also helpful predict the locations of landslides triggered by subsequent events, e.g. strong aftershocks and rainfalls, which would be a scientific reference for restoration, reconstruction, and landslide reduction and mitigation in the Gorkha earthquake-affected area.

#### Acknowledgments

This research was supported by the National Natural Science Foundation of China (41661144037, 41472202, 41472264) and the Special Project for China Earthquake Research (201508024). We are very grateful to the comments of two anonymous reviewers and the help of Ranjan Kumar Dahal (Editor).

#### Competing interests

The authors declare that they have no competing interests.

#### Authors' contributions

CX and YT mapped landslides on GE images. CX and GL participated the field investigations. CX, BZ, and HR provided the regional geologic and tectonic data. CX drafted the manuscript. All the authors reviewed and approved the manuscript.

#### Publisher's Note

Springer Nature remains neutral with regard to jurisdictional claims in published maps and institutional affiliations.

#### Author details

<sup>1</sup>Key Laboratory of Active Tectonics and Volcano, Institute of Geology, China Earthquake Administration, 1# Huayuanli, Chaoyang District, PO Box 9803, Beijing 100029, China. <sup>2</sup>CCCC Highway Consultants Co., Ltd., Beijing 100088, China.

Received: 9 August 2016 Accepted: 30 March 2017

Published online: 05 April 2017

#### References

- Angster, S., E.J. Fielding, S. Wesnousky, I. Pierce, D. Chamlagain, D. Gautam, B.N. Upreti, Y. Kumahara, and T. Nakata. 2015. Field reconnaissance after the 25 April 2015 M 7.8 Gorkha earthquake. *Seismological Research Letters* 86(6): 1506–1513. doi:10.1785/0220150135.
- Avouac, J.-P., L. Meng, S. Wei, T. Wang, and J.-P. Ampuero. 2015. Lower edge of locked main Himalayan Thrust unzipped by the 2015 Gorkha earthquake. *Nature Geoscience* 8: 701–711. doi:10.1038/ngeo2518.
- British Geological Survey, Earthquakes without Frontiers, Durham University. 2015. *2015 Nepal Earthquakes mapped landslide intensity (Revision 4.0 - 19 June 2015)*. <https://data.hdx.rwllabs.org/group/nepal-earthquake>.
- Collins, B.D., and R.W. Jibson. 2015. *Assessment of existing and potential landslide hazards resulting from the April 25, 2015 Gorkha, Nepal earthquake sequence*. US Geological Survey. <https://pubs.er.usgs.gov/publication/ofr20151142>. doi:10.3133/ofr20151142.
- Dahal, R.K. 2016. Initiatives for rockfall hazard mitigation in Nepal. *Bulletin of Nepal Geological Society* 33: 51–56.
- Duputel, Z., J. Vergne, L. Rivera, G. Wittlinger, V. Farra, and G. Hetényi. 2016. The 2015 Gorkha earthquake: a large event illuminating the main Himalayan thrust fault. *Geophysical Research Letters* 43(6): 2517–2525. doi:10.1002/2016GL068083.
- Elliott, J.R., R. Jolivet, P.J. González, J.-P. Avouac, J. Hollingsworth, M.P. Searle, and V.L. Stevens. 2016. Himalayan megathrust geometry and relation to topography revealed by the Gorkha earthquake. *Nature Geoscience* 9: 174–180. doi:10.1038/ngeo2623.
- Feng, H., A. Zhou, J. Yu, X. Tang, J. Zheng, X. Chen, and S. You. 2016. A comparative study on plum-rain-triggered landslide susceptibility assessment models in West Zhejiang Province. *Earth Science* 41(3): 403–415.
- Gnyawali, K.R., S. Maka, B.R. Adhikari, D. Chamlagain, S. Duwal, and A.R. Dhungana. 2016. Spatial implications of earthquake induced landslides triggered by the April 25 Gorkha earthquake Mw 7.8: preliminary analysis and findings. In *International conference on earthquake engineering and post disaster reconstruction planning 24 – 26 April, 2016, Bhaktapur, Nepal*, 50–58.
- Gorum, T., O. Korup, C.J. van Westen, M. van der Meijde, C. Xu, and F.D. van der Meer. 2014. Why so few? Landslides triggered by the 2002 Denali earthquake, Alaska. *Quaternary Science Reviews* 95: 80–94. doi:10.1016/j.quascirev.2014.04.032.
- Hashash, Y.M.A., B. Tiwari, R.E.S. Moss, D. Asimaki, K.B. Clahan, D.S. Kieffer, D.S. Dreger, A. Macdonald, C.M. Madugo, H.B. Mason, M. Pehlivan, D. Rayamajhi, I. Acharya, and B. Adhikari. 2015. Geotechnical field reconnaissance: Gorkha (Nepal) earthquake of April 25, 2015 and related shaking sequence. In *Geotechnical extreme event reconnaissance GEER association report No. GEER-040*. <https://works.bepress.com/rmoss/47/>: 250 pages.
- Kargel JS, Leonard GJ, Shugar DH, Haritashya UK, Bevington A, Fielding EJ, Fujita K, Geertsema M, Miles ES, Steiner J, Anderson E, Bajracharya S, Bawden GW, Breashears DF, Byers A, Collins B, Dhital MR, Donnellan A, Evans TL, Geai ML, Glasscoe MT, Green D, Gurung DR, Heijnen R, Hilborn A, Hudnut K, Huyck C, Immerzeel WW, Jiang L, Jibson R, Käb A, Khanal NR, Kirschbaum D, Kraaijenbrink PDA, Lamsal D, Liu S, Lv M, McKinney D, Nahirnick NK, Nan Z, Ojha S, Olsenholler J, Painter TH, Pleasants M, Pratima KC, Qi Y, Raup BH, Regmi D, Rounce DR, Sakai A, Shangguan D, Shea JM, Shrestha AB, Shukla A, Stumm D, van der Kooij M, Voss K, Wang X, Weihs B, Wolfe D, Wu L, Yao X, Yoder MR, Young N. 2016. Geomorphic and geologic controls of geohazards induced by Nepal's 2015 Gorkha earthquake. *Science* 351(6269): aac8353. doi:10.1126/science.aac8353
- Koketsu, K., H. Miyake, Y. Guo, H. Kobayashi, T. Masuda, S. Davuluri, M. Bhattarai, L. B. Adhikari, and S.N. Sapkota. 2016. Widespread ground motion distribution caused by rupture directivity during the 2015 Gorkha, Nepal earthquake. *Scientific Reports* 6: 28536. doi:10.1038/srep28536.
- Lacroix, P. 2016. Landslides triggered by the Gorkha earthquake in the Langtang valley, volumes and initiation processes. *Earth, Planets and Space* 68(1): 46. doi:10.1186/s40623-016-0423-3.
- Larsen, I.J., D.R. Montgomery, and O. Korup. 2010. Landslide erosion controlled by hillslope material. *Nature Geoscience* 3(4): 247–251. doi:10.1038/ngeo776.
- Le Fort, P. 1975. Himalayas: the collided range. Present knowledge of the continental arc. *American Journal of Science* 275-A: 1–44.
- Lee, C.T., C.C. Huang, J.F. Lee, K.L. Pan, M.L. Lin, and J.J. Dong. 2008. Statistical approach to earthquake-induced landslide susceptibility. *Engineering Geology* 100(1–2): 43–58. doi:10.1016/j.enggeo.2008.03.004.
- Martha TR, Roy P, Mazumdar R, Govindharaj KB, Kumar KV. 2016. Spatial characteristics of landslides triggered by the 2015 Mw 7.8 (Gorkha) and Mw 7.3 (Dolakha) earthquakes in Nepal. Landslides. doi:10.1007/s10346-016-0763-x
- Moss, R.E.S., E.M. Thompson, D.S. Kieffer, B. Tiwari, Y.M.A. Hashash, I. Acharya, B.R. Adhikari, D. Asimaki, K.B. Clahan, and B.D. Collins. 2015. Geotechnical effects of the 2015 magnitude 7.8 Gorkha, Nepal, earthquake and aftershocks. *Seismological Research Letters* 86(6): 1514–1523. doi:10.1785/0220150158.
- Mukherjee, S. 2015. A review on out-of-sequence deformation in the Himalaya. *Geological Society, London, Special Publications* 412(S): 67–109. doi:10.1144/SP412.13.



- Nakata, T. 1989. Active faults of the Himalaya of India and Nepal. *Geological Society of America Special Papers* 232: 243–264. doi:10.1130/SPE232-p243.
- Parameswaran, R.M., T. Natarajan, K. Rajendran, C.P. Rajendran, R. Mallick, M. Wood, and H.C. Lekhak. 2015. Seismotectonics of the April-May 2015 Nepal earthquakes: An assessment based on the aftershock patterns, surface effects and deformational characteristics. *Journal of Asian Earth Sciences* 111: 161–174. doi:10.1016/j.jseas.2015.07.030.
- Pathak, D. 2016. Knowledge based landslide susceptibility mapping in the Himalayas. *Geoenvironmental Disasters* 3(1): 8. doi:10.1186/s40677-016-0042-0.
- Sarkar, S., D.P. Kanungo, A.K. Patra, and P. Kumar. 2008. GIS based spatial data analysis for landslide susceptibility mapping. *Journal of Mountain Science* 5(1): 52–62. doi:10.1007/s11629-008-0052-9.
- Sharma, K., L. Deng, and C.C. Noguez. 2016. Field investigation on the performance of building structures during the April 25, 2015, Gorkha earthquake in Nepal. *Engineering Structures* 121: 61–74. doi:10.1016/j.engstruct.2016.04.043.
- Shen, L., C. Xu, and L. Liu. 2016. Interaction among controlling factors for landslides triggered by the 2008 Wenchuan, China Mw 7.9 earthquake. *Frontiers of Earth Science* 10(2): 264–273. doi:10.1007/s11707-015-0517-4.
- Sun, B., and P. Yan. 2015. Damage characteristics and seismic capacity of buildings during Nepal Ms 8.1 earthquake. *Earthquake Engineering and Engineering Vibration* 14(3): 571–578. doi:10.1007/s11803-015-0046-x.
- Tian, Y., C. Xu, X. Xu, and J. Chen. 2016. Detailed inventory mapping and spatial analyses to landslides induced by the 2013 Ms 6.6 Minxian earthquake of China. *Journal of Earth Science* 27(6): 1016–1026. doi:10.1007/s12583-016-0905-z.
- Tsangaratos, P., and I. Ilia. 2016. Comparison of a logistic regression and Naïve Bayes classifier in landslide susceptibility assessments: The influence of models complexity and training dataset size. *Catena* 145: 164–179. doi:10.1016/j.catena.2016.06.004.
- Upreti, B.N. 1999. An overview of the stratigraphy and tectonics of the Nepal Himalaya. *Journal of Asian Earth Sciences* 17(5-6): 577–606. doi:10.1016/S1367-9120(99)00047-4.
- Wang, K., and Y. Fialko. 2015. Slip model of the 2015 Mw 7.8 Gorkha (Nepal) earthquake from inversions of ALOS-2 and GPS data. *Geophysical Research Letters* 42(18): 7452–7458. doi:10.1002/2015GL065201.
- Wang, F., M. Miyajima, R. Dahal, M. Timilsina, T. Li, M. Fujiu, Y. Kuwada, and Q. Zhao. 2016. Effects of topographic and geological features on building damage caused by 2015.4.25 Mw7.8 Gorkha earthquake in Nepal: a preliminary investigation report. *Geoenvironmental Disasters* 3(1): 7. doi:10.1186/s40677-016-0040-2.
- Wesnousky, S.G., S. Kumar, R. Mohindra, and V. Thakur. 1999. Uplift and convergence along the Himalayan Frontal Thrust of India. *Tectonics* 18(6): 967–976. doi:10.1029/1999TC900026.
- Xu, C. 2015. Preparation of earthquake-triggered landslide inventory maps using remote sensing and GIS technologies: principles and case studies. *Geoscience Frontiers* 6(6): 825–836. doi:10.1016/j.gsf.2014.03.004.
- Xu, C., X. Xu, F. Dai, and A.K. Saraf. 2012. Comparison of different models for susceptibility mapping of earthquake triggered landslides related with the 2008 Wenchuan earthquake in China. *Computers & Geosciences* 46: 317–329. doi:10.1016/j.cageo.2012.01.002.
- Xu C, Xu X, Dai F, Wu Z, He H, Wu X, Xu S, Shi F. 2013a. Application of an incomplete landslide inventory, logistic regression model and its validation for landslide susceptibility mapping related to the May 12, 2008 Wenchuan earthquake of China. *Natural Hazards* 68(2): 883-900. doi:10.1007/s11069-013-0661-7.
- Xu C, Xu X, Yao Q, Wang Y. 2013b. GIS-based bivariate statistical modelling for earthquake-triggered landslides susceptibility mapping related to the 2008 Wenchuan earthquake, China. *Quarterly Journal of Engineering Geology and Hydrogeology* 46(2): 221-236. doi:10.1144/qjgeh2012-006.
- Xu, C., X. Xu, X. Yao, and F. Dai. 2014. Three (nearly) complete inventories of landslides triggered by the May 12, 2008 Wenchuan Mw 7.9 earthquake of China and their spatial distribution statistical analysis. *Landslides* 11(3): 441–461. doi:10.1007/s10346-013-0404-6.
- Xu, C., X. Xu, and J.B.H. Shyu. 2015. Database and spatial distribution of landslides triggered by the Lushan, China Mw 6.6 earthquake of 20 April 2013. *Geomorphology* 248: 77–92. doi:10.1016/j.geomorph.2015.07.002.
- Xu C, Xu X, Tian Y, Shen L, Yao Q, Huang X, Ma J, Chen X, Ma S. 2016a. Two comparable earthquakes produced greatly different coseismic landslides: The 2015 Gorkha, Nepal and 2008 Wenchuan, China events. *Journal of Earth Science* 27(6): 1008-1015. doi:10.1007/s12583-016-0684-6.
- Xu C, Xu X, Shen L, Yao Q, Tan X, Kang W, Ma S, Wu X, Cai J, Gao M, Li K. 2016b. Optimized volume models of earthquake-triggered landslides. *Scientific Reports* 6: 29797. doi:10.1038/srep29797.
- Yalcin, A. 2008. GIS-based landslide susceptibility mapping using analytical hierarchy process and bivariate statistics in Ardesen (Turkey): Comparisons of results and confirmations. *Catena* 72(1): 1–12. doi:10.1016/j.catena.2007.01.003.

**Submit your manuscript to a SpringerOpen® journal and benefit from:**

- Convenient online submission
- Rigorous peer review
- Immediate publication on acceptance
- Open access: articles freely available online
- High visibility within the field
- Retaining the copyright to your article

Submit your next manuscript at ► [springeropen.com](http://springeropen.com)